

Topology Optimization of Magnetically-Loaded Planar Inverted-F Antenna for Handset

[#]Naobumi Michishita, Shinya Endoh and Hisashi Morishita

Department of Electrical and Electronic Engineering, National Defense Academy
1-10-20 Hashirimizu, Yokosuka, 239-8686 Japan, naobumi@nda.ac.jp

1. Introduction

The combined method of the topology optimization and the finite-difference time-domain (FDTD) method has been proposed for bandwidth enhancement of dielectric resonator antenna [1]. The objective function is the integral value of the reflection pulse from the feed point to the coaxial line. The topology of the dielectric material is optimized to minimize the objective function. As a result, the bandwidth becomes four times wider than the initial homogeneous material.

The topology optimization method (TOM) has been applied to optimize the configuration and arrangement of the magnetic materials for miniaturization of the planar inverted-F antenna (PIFA) on the infinite ground plane [2],[3] and the enclosure for a handset [4]. However, the dielectric and magnetic effects and the validity of the optimized topologies of the magnetic materials are not cleared.

In this paper, the configuration and the arrangement of the magnetic materials for miniaturization of the PIFA are investigated. The effects of the dielectric and magnetic materials and their amounts depend on the arranging position of the magnetic materials. The design region by using TOM for the implementation of the magnetic materials causes the various optimized topologies of the magnetic materials. The VSWR and radiation characteristics of the optimized magnetically-loaded PIFA are verified through finite element method (FEM) and measured results of the simplified configuration of the magnetic materials.

2. Implementation Effects of Dielectric and Magnetic Materials

The analytic model of the PIFA on the conducting box is shown in Fig. 1. The 12-mm-square patch with 0.2 mm thickness is located on the upper-left corner of the conducting box. The magnetic materials can be implemented in the area between PIFA and the conducting box. The coaxial cable is modelled for exciting the PIFA. The locations of the feed and short pins are adjusted for the impedance matching. Fig. 2 shows the back view of the PIFA with the magnetic materials in order to examine the implementation effects of dielectric and magnetic materials. The Model A and B are the implementation of the magnetic materials with 2 mm width in the bottom and upper parts of the PIFA, respectively. Fig. 3(a) shows the VSWR characteristics of Model A with $h = 6$ mm when ϵ_r and μ_r are varied. The simulated results are obtained by FEM. The resonant frequency of the PIFA with high ϵ_r materials becomes lower frequency, and the magnetic material has only a small effect in the bottom part of the PIFA. Fig. 3(b) shows the VSWR characteristics of Model B with $h = 6$ mm when ϵ_r and μ_r are varied. The resonant frequency of the PIFA with high μ_r materials becomes lower frequency, and the impedance matching can be maintained in the upper part of the PIFA. Fig. 4(a) shows the VSWR characteristics of Model A with $\epsilon_r = 20$ and $\mu_r = 1$ when h is varied. The amount of the dielectric materials affects the resonant frequency and impedance matching in the bottom part of the PIFA. Fig. 4(b) shows the VSWR characteristics of Model B with $\epsilon_r = 1$ and $\mu_r = 10$ when h is varied. The resonant frequency monotonically decreases when h becomes small, and the impedance matching does not depend on h . The effect of the amount of the magnetic materials depends on the electromagnetic distributions between the PIFA and the conducting box.

3. Topology Optimized PIFA with Magnetic Materials

Fig. 5 shows an antenna model with a design region to use for TOM. The design region between the PIFA and the conducting box is composed of magnetic materials with $\epsilon_r = 13.0$, $\mu_r = 2.5$, $\tan\delta_\epsilon = 0.01$, $\tan\delta_\mu = 0.06$. The FDTD method is used for electromagnetic analysis, and the design region is discretized using Yee cells. The relative permittivity and permeability are controlled by normalized density in the design region. The reflection pulse is obtained by subtracting the incident pulse from the observed pulse in the coaxial cable with 2 by 2 cells. The objective function is the reflection power in the frequency range around the desired frequency, which corresponds to the modulation frequency and the half power bandwidth of the input Gaussian pulse. If the objective function does not converge, the design sensitivity is obtained by the adjoint variable method, and the design variables are updated using the sequential linear programming. Fig. 6(a) shows the optimized configuration of the magnetic materials by using TOM when $a = b = 12$ mm. Fig. 6(b) shows the simplified configuration of the magnetic material for FEM and experiment. The amount of the magnetic materials is 248 mm^3 . Figs. 7 and 8 show the VSWR and radiation characteristics. The FEM results are in good agreement with measured results. The discrepancy of the FEM and FDTD results is due to the simplification of the magnetic materials. The antenna size is 38.3% of the PIFA without the magnetic materials and the radiation efficiency at 2.1 GHz is 84.8%. The optimized topology of the magnetic materials is different from the previous results in the design region with $a = 12$, $b = 16$ [4]. In the case of $a = 12$, $b = 16$, the antenna size was 49.4% by using TOM. Therefore, the amount of the magnetic materials depends on the design region. It is required careful modeling of the edge of the PIFA, because Yee's algorithm cannot evaluate the electric and magnetic components at one discrete node at the same time.

4. Conclusion

The miniaturization of the magnetically-loaded PIFA has been investigated by using TOM. The effects of the dielectric and magnetic materials and their amounts depend on the arranging position of the magnetic materials. The miniaturization of the PIFA can be realized by limiting the design region of the magnetic materials between the PIFA and the conducting box. The VSWR and the radiation characteristics are confirmed in the experiment.

Acknowledgments

The authors wish to acknowledge the support from Dr. Tsuyoshi Nomura and Dr. Kazuo Sato, Toyota Central R&D Laboratories, Inc. for using the topology design optimization.

References

- [1] T. Nomura and K. Sato, "Topology Design Optimization of Dielectric Resonator Antennas Using Finite-Difference Time-Domain Method," IEEE AP-S International Symposium, pp.1317-1320, July 2006.
- [2] A. Matsuzaki, H. Morishita, T. Nomura, K. Sato, K. Taguchi and T. Kashiwa, "Topology Optimization of PIFA Loaded with Magnetic Material by Using FDTD Method," IEEE AP-S International Symposium, pp.605-608, July 2006.
- [3] A. Matsuzaki, H. Morishita, T. Nomura and K. Sato, "Miniaturization of Built-in Antenna Loaded with Magnetic Materials for Handset by Using Topology Optimization," International Symposium on Antennas and Propagation, a180_r218, pp.1-4, Nov. 2006.
- [4] A. Matsuzaki, S. Endoh, H. Morishita, T. Nomura and K. Sato, "A Study on Miniaturization of Antenna Loaded with Magnetic Materials by Using Topology Optimization," IEEE AP-S International Symposium, pp.2602-2605, June 2007.

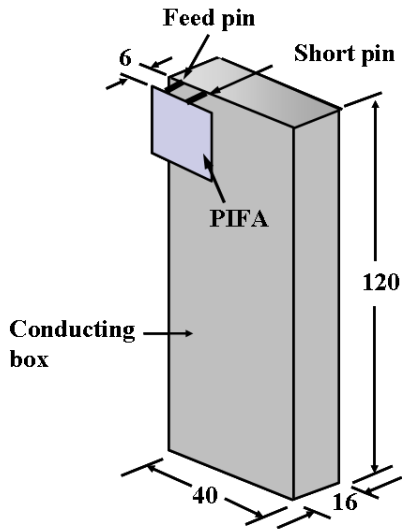


Fig. 1. PIFA installed on conducting box.

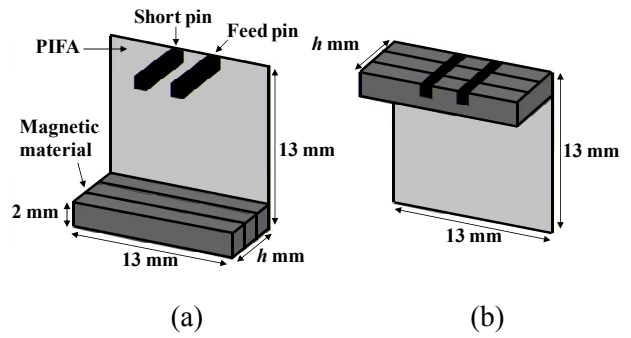
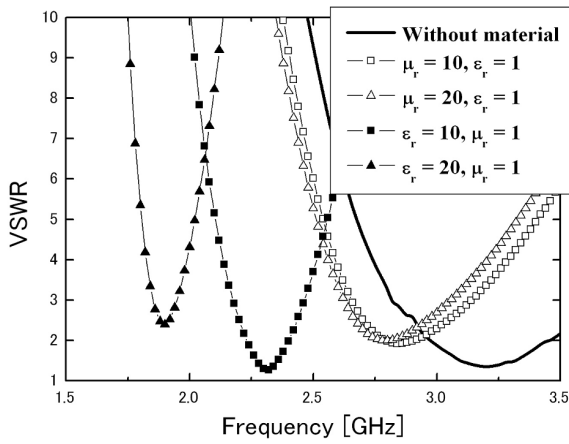
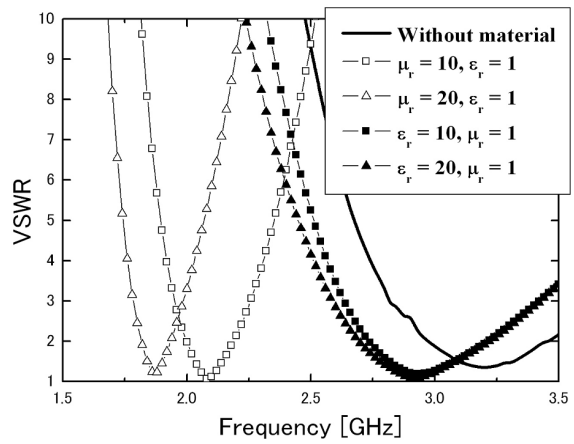


Fig. 2. PIFA loaded with magnetic material. (a) Model A. (b) Model B.

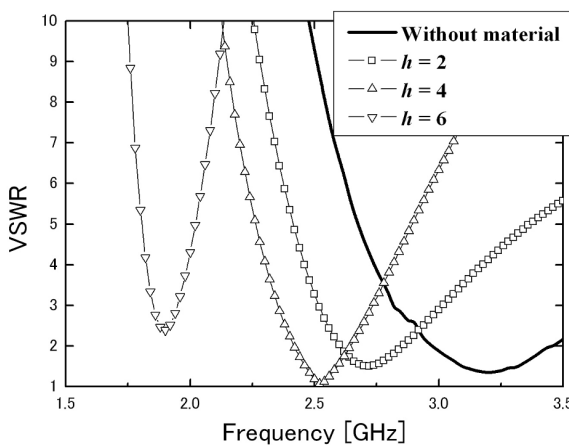


(a)

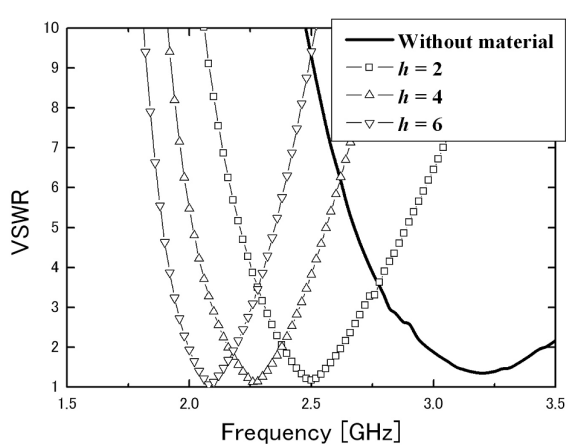


(b)

Fig. 3. VSWR characteristics when ϵ_r and μ_r are varied at $h = 6$ mm. (a) Model A. (b) Model B.



(a)



(b)

Fig. 4. VSWR characteristics when h is varied. (a) Model A. $\epsilon_r = 20, \mu_r = 1$. (b) Model B. $\epsilon_r = 1, \mu_r = 10$.

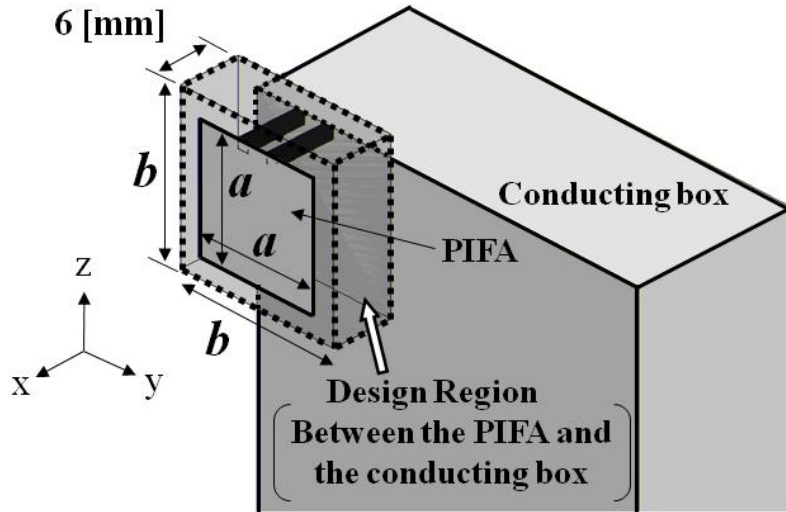


Fig. 5. Analytic model for TOM. The design space is located between PIFA and conducting box.

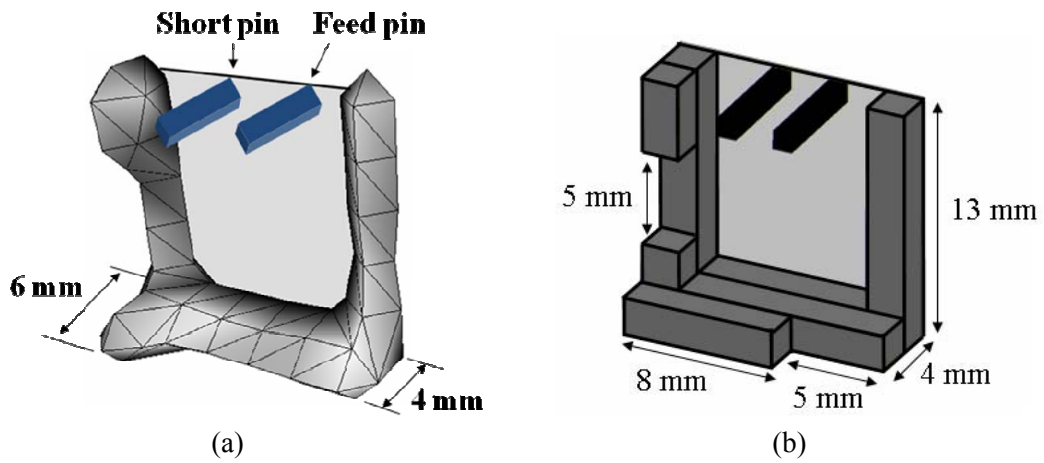


Fig. 6. Configurations of magnetic materials in the design space. (a) Optimum configuration of magnetic material by using TOM. (b) Simple model for FEM simulator.

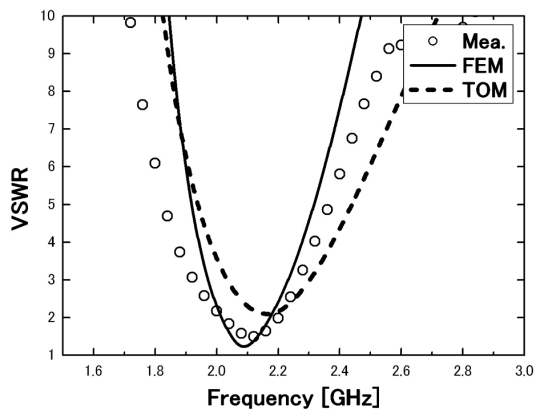


Fig. 7. VSWR characteristics

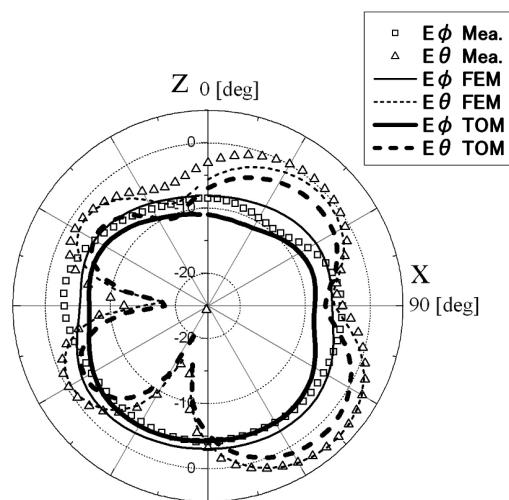


Fig. 8. Radiation Patterns